

NMR structure-based optimization of *Staphylococcus aureus* sortase A pyridazinone inhibitors

Albert H. Chan^{1,2,3}  | Sung Wook Yi¹ | Ethan M. Weiner^{1,2,3} | Brendan R. Amer^{1,2,3} | Christopher K. Sue¹ | Jeff Wereszczynski⁴ | Carly A. Dillen⁵ | Silvia Senese¹ | Jorge Z. Torres¹ | J. Andrew McCammon^{6,7,8} | Lloyd S. Miller⁵ | Michael E. Jung¹ | Robert T. Clubb^{1,2,3}

¹Department of Chemistry and Biochemistry, University of California, Los Angeles, Los Angeles, CA, USA

²UCLA-DOE Institute of Genomics and Proteomics, University of California, Los Angeles, Los Angeles, CA, USA

³Molecular Biology Institute, University of California, Los Angeles, Los Angeles, CA, USA

⁴Department of Physics and Center for Molecular Study of Condensed Soft Matter, Illinois Institute of Technology, Chicago, IL, USA

⁵Department of Dermatology, Johns Hopkins University School of Medicine, Baltimore, MD, USA

⁶Department of Chemistry and Biochemistry, University of California, San Diego, La Jolla, CA, USA

⁷Howard Hughes Medical Institute, University of California, San Diego, La Jolla, CA, USA

⁸Department of Pharmacology, University of California, San Diego, La Jolla, CA, USA

Correspondence

Robert T. Clubb and Michael E. Jung, Department of Chemistry and Biochemistry, University of California, Los Angeles, Los Angeles, CA, USA.

Emails: rclubb@mbi.ucla.edu; jung@chem.ucla.edu.

Funding information

National Institute of Allergy and Infectious Diseases, Grant/Award Number: AI52217; National Institute of General Medical Sciences, Grant/Award Number: GM008496 and GM31749

Staphylococcus aureus is a leading cause of hospital-acquired infections in the USA and is a major health concern as methicillin-resistant *S. aureus* and other antibiotic-resistant strains are common. Compounds that inhibit the *S. aureus* sortase (SrtA) cysteine transpeptidase may function as potent anti-infective agents as this enzyme attaches virulence factors to the bacterial cell wall. While a variety of SrtA inhibitors have been discovered, the vast majority of these small molecules have not been optimized using structure-based approaches. Here we have used NMR spectroscopy to determine the molecular basis through which pyridazinone-based small molecules inhibit SrtA. These inhibitors covalently modify the active cysteine thiol and partially mimic the natural substrate of SrtA by inducing the closure of an active site loop. Computational and synthetic chemistry methods led to second-generation analogues that are ~70-fold more potent than the lead molecule. These optimized molecules exhibit broad-spectrum activity against other types of class A sortases, have reduced cytotoxicity, and impair SrtA-mediated protein display on *S. aureus* cell surface. Our work shows that pyridazinone analogues are attractive candidates for further development into anti-infective agents, and highlights the utility of employing NMR spectroscopy and solubility-optimized small molecules in structure-based drug discovery.

KEYWORDS

molecular docking, molecular dynamics, NMR, protein structure, protein-inhibitor complex, Sortase, SrtA, *Staphylococcus aureus*, transpeptidase

Abbreviations: AAEEK, aryl (β -amino)ethyl ketone; Ba-SrtA, *Bacillus anthracis* sortase A; Ba-SrtB, *Bacillus anthracis* sortase B; MRSA, methicillin-resistant *Staphylococcus aureus*; SrtA, *Staphylococcus aureus* sortase A.

1 | INTRODUCTION

Staphylococcus aureus is a leading cause of hospital- and community-acquired infections in the USA. This bacterial pathogen is estimated to cause 11,000 deaths annually in the USA. It inflicts a wide range of life-threatening diseases such as pneumonia, meningitis, osteomyelitis, endocarditis, toxic shock syndrome, bacteremia, and sepsis.^{[1]a} *S. aureus* skin and soft tissue infections also represent a major clinical problem as they result in over 11 million outpatient and emergency room visits, and close to 500,000 hospital admissions per year in the USA.^[2,3] The rise of methicillin-resistant *S. aureus* (MRSA) is a major health problem that has created a pressing need for new antibiotics. MRSA harbors genes that confer resistance to β -lactam antibiotics and is now endemic in hospitals. *S. aureus* has also developed resistance to other antibiotics, including last resort and newer generation drugs, such as vancomycin, daptomycin, and linezolid.^[4–6] The *S. aureus* sortase A (SrtA) enzyme is an attractive molecular target for the development of novel antibiotics. This is because this enzyme covalently attaches a range of protein virulence factors to the surface of *S. aureus* that play critical roles in the infection process, including promoting bacterial adhesion to host tissues, acquisition of essential nutrients, and the evasion and suppression of the immune response.^[7,8] Several studies have shown that *srtA*[−] *S. aureus* mutants have reduced virulence in animal models of infection, presumably because their surfaces are devoid of key protein factors required to colonize host tissue and evade the immune response.^[9,10] SrtA-related enzymes are also used by other clinically important pathogens to display factors that are required for their virulence (e.g., *Enterococcus faecilis*, *Listeria monocytogenes*, *Bacillus anthracis*, *Streptococcus pyogenes*, and *Streptococcus pneumoniae*).^[10] Thus, small-molecule SrtA enzyme inhibitors could function as potent anti-infective agents to treat MRSA and infections caused by other types of Gram-positive bacteria.

SrtA resides on the extracellular membrane where it covalently attaches proteins to peptidoglycan by catalyzing a transpeptidation that joins proteins containing a C-terminal cell wall sorting signal (CWSS) to the cross-bridge peptide.^[11] Besides its important role in pathogenesis, SrtA has several other properties that make it an attractive drug target: (i) It has no human homolog, reducing the likelihood of off-target effects, (ii) it is located on the bacterial surface such that inhibitors do not need to cross the cell membrane, thereby reducing potential cytotoxicity, and (iii) it is not required for the growth of *S. aureus* and other clinically important microbes when they are outside their human host.^[12] Therefore, SrtA inhibitors that selectively target virulence mechanisms could have a distinct advantage over conventional antibiotics, as they may not induce the same selective pressures that lead to drug resistance.^[13,14]

Several research groups have sought to identify small-molecule SrtA inhibitors that could be developed into therapeutics.^[10,15] The small molecules that have thus far been identified include natural products and synthetic molecules identified by screening compound libraries, and rationally designed molecules that mimic the substrate or transition state intermediates.^[10] In addition, virtual screening methods have been employed to identify inhibitors using the structure of the apo- or substrate-bound forms of the enzyme.^[10] However, a clinically useful SrtA inhibitor has yet to be developed. A major obstacle hindering drug development has been the difficulty in applying structure-based methods to optimize SrtA inhibitors. This is because the active site of SrtA is structurally disordered in its apo-state making it difficult to model drug–enzyme interactions computationally and potentially hindering the application of X-ray crystallography that require crystallization of the SrtA–inhibitor complex. At present, only Zhulenkov and colleagues have used NMR spectroscopy to visualize how SrtA binds to an inhibitor, a benzisothiazolinone-based small molecule that irreversibly modifies the enzyme.^[16] However, the structure of the inhibitor–SrtA complex was determined at low resolution. Maresso, et al. have also structurally characterized covalent inhibitors of the aryl (β -amino)ethyl ketone class by co-crystallizing the inhibitors with the sortase B from *Bacillus anthracis* (Ba-SrtB).^[17] However, Ba-SrtB may not be a good platform from which to optimize *S. aureus* SrtA inhibitors, as SrtA and Ba-SrtB have distinct active site structures and recognize different sorting signal substrates; SrtA and Ba-SrtA recognize LPXTG and NPQTN sorting signals, respectively.^[18] Thus, while many compounds inhibit the activity of SrtA in vitro, a lack of structural data to rationally optimize these molecules for clinical applications has been problematic.

Using high-throughput screening (HTS) methods, we previously identified pyridazinone-based molecules that are potent inhibitors of SrtA.^[19] However, these molecules were not optimized using structure-based approaches because they were poorly soluble in water, which made it difficult to experimentally determine the three-dimensional structure of the enzyme–inhibitor complex, and because conformational disorder in the SrtA's active site made it difficult to computationally model enzyme–inhibitor interactions. We have now overcome this problem using a highly soluble pyridazinone analogue whose complex with SrtA could be determined using NMR spectroscopy. We show that pyridazinone inhibitors partially mimic the natural substrate, by inducing a conformational change in the active site that incompletely closes a key active site loop, resulting in a final structure that is reminiscent of both the apo- and sorting signal-bound forms of the enzyme. Guided by computational studies of the complex, a series of pyridazinone analogues were synthesized and their efficacy evaluated in vitro and in cell culture. This

work led to the discovery of 2-(3-fluorophenyl)-4-(3-hydroxypropoxy)-5-mercaptopyridazin-3(2H)-one, which inhibits SrtA-mediated protein display in *S. aureus* and improves inhibitory activity over the lead molecule 70-fold (IC_{50} value of 21 ± 14 nM). The use of a solubility-optimized inhibitor analogue for NMR studies of the complex was critical and may be a generally useful strategy to study other enzyme inhibitor interactions.

2 | METHODS AND MATERIALS

2.1 | Preparation of the SrtA–inhibitor complex for NMR and mass spectrometry studies

The catalytic domain of SrtA (residues Gln⁶⁰-Lys²⁰⁶) was prepared as described previously.^[20] To form a SrtA:inhibitor complex, 0.5 mM uniformly ¹⁵N- and ¹³C-labeled SrtA was incubated with 5 mM of sodium thiolate 4-ethoxy-5-mercapto-2-phenylpyridazin-3(2H)-one (hereafter referred as **2-salt**) in 50 mM Tris, pH 6.4, 150 mM NaCl, 20 mM CaCl₂ for 72 hr at room temperature. The complex was then dialyzed into NMR buffer that consisted of 50 mM Tris, pH 6.4, 150 mM NaCl, and 20 mM CaCl₂. Two NMR samples were studied that each contained 1.5 mM SrtA–inhibitor complex dissolved NMR buffer and either 7% or 99.999% D₂O. Mass spectrometry was used to verify that the inhibitor forms a disulfide bond with Cys¹⁸⁴ in SrtA. The SrtA:**2-salt** complex was first digested with trypsin by incubating 20 μM ¹⁵N/¹³C-SrtA:**2-salt** complex with 5 μg/ml trypsin for 24 hr at 37°C. The digestion reaction mixture was then split into two aliquots. To one of the aliquots, DTT was added to a final concentration of 5 mM. Both aliquots were then subjected to LC-MS analysis to monitor the masses of the cleaved peptides. LC-MS experiments were carried out on a Waters Acquity UPLC connected to a Waters LCT-Premier XE Time of Flight Instrument controlled by MASSLYNX 4.1 software (Waters Corp., Milford, MA, USA). Digested protein samples in 20 mM HEPES and 5 mM CaCl₂ were separated using an Phenomenex Hydro-RP column (3.0 × 50 mm, 4 μm packing) and were eluted with a gradient of 2%–50% solvent B over 10 min using a flow rate of 0.425 ml/min (solvent A: water, solvent B: acetonitrile, both with 0.3% formic acid). The mass spectrometer was equipped with a multimode source operated in the electrospray mode. Mass spectra were recorded from a mass of 70–2,000 Da. Capillary voltage was set to 1700 V and the source/desolvation gas temperatures were 120°C/350°C, respectively. The ion abundance values for product ions at *m/z* 819.5, 942.5, 1638, and 1886 were monitored by generating extracted ion chromatograms using a 0.5-Da mass window and integrating the peaks of interest. These ions had retention time values of 5.09, 6.86, 5.09, and 6.86 min, respectively.

2.2 | NMR spectroscopy and structure determination

NMR spectra of the SrtA:inhibitor complex were acquired at 298 K on Bruker Avance 500-, 600-, and 800-MHz spectrometers equipped with triple resonance cryogenic probes. NMR spectra were processed using NMRPipe^[21] and analyzed using the PIPP^[22] and CARRA (version 1.8.4)^[23] software packages. Chemical shift assignments (¹H, ¹³C, ¹⁵N) of SrtA were obtained by analyzing the following experiments: HNCA, HNCACB, CBCA(CO)NH, HNCO, HN(CA)CO, ¹⁵N-edited TOCSY, HNHA, HNHB, HBHA(CO)NH, HCCH-TOCSY, HCCH-COSY, (HB)CB(CGCDCE)HE, and (HB)CB(CGCD)HD (reviewed in^[24,25]). Chemical shift assignments for the inhibitor were obtained by analyzing a two-dimensional (F2) ¹³C-filtered NOESY spectrum. The majority of ϕ and ψ dihedral angle restraints were obtained using the program TALOS+.^[26] Additional backbone ϕ angle restraints were obtained by analyzing HNHA spectra.^[27] Intramolecular protein distance restraints were obtained from three-dimensional ¹⁵N- and ¹³C-edited NOESY spectra. Intermolecular distance restraints were obtained by analyzing two-dimensional (F2) ¹³C-filtered NOESY and ¹³C-edited NOESY-HSQC spectra of the complex.

NOE assignments were initially obtained automatically using the programs ATNOS/CANDID controlled by UNIO^[28,29] utilizing XPLOR-NIH (version 2.23).^[30] NOE assignments were then verified manually for the active site residues (Val¹⁶¹-Asp¹⁷⁵ [$\beta 6/\beta 7$ loop], Thr¹⁸³-Lys¹⁹⁶ [$\beta 7/\beta 8$ loop], and side chains of Leu⁹⁷, Ser¹¹⁶, His¹²⁰, Thr¹⁸⁰, Ile¹⁸², and Val²⁰¹) by inspecting the NOESY data. During inspection of the NOESY data, additional NOE restraints involving active site residues were identified and included in subsequent structure calculations. Final structures were calculated using XPLOR-NIH based on the lowest energy conformer of the previously solved apo-SrtA NMR structure (PDB 1IJA).^[20] During the course of the structure calculations, backbone and side chain atoms of active site residues Val¹⁶¹-Asp¹⁷⁵ ($\beta 6/\beta 7$ loop) and Thr¹⁸³-Lys¹⁹⁶ ($\beta 7/\beta 8$ loop), as well as side chain atoms of Leu⁹⁷, Ser¹¹⁶, His¹²⁰, Thr¹⁸⁰, Ile¹⁸², Arg¹⁹⁷, Ile¹⁹⁹, and Val²⁰¹, were allowed to move while all other SrtA atoms were held fixed in space. Residues within the $\beta 6/\beta 7$ and $\beta 7/\beta 8$ loops were allowed to move because they form the surface surrounding the presumed inhibitor binding site, and previous crystal and NMR structural studies of apo- and substrate (LPAT*)-bound SrtA reveal these loops adopt distinct conformations as a result of substrate binding.^[20,31,32] Mobility of other active site residues was restricted to their side chains because while they make contacts with the sorting signal substrate in the SrtA:LPAT* structure, they do not demonstrate significant backbone rearrangement. Non-active site residues were kept rigid because they show little difference (RMSD = 0.8 Å) between the apo- and substrate-bound SrtA

structures, and such structural information is of little value for structure-based drug design of a competitive inhibitor. In the final set of calculations, a thiol group within the inhibitor was attached to Cys¹⁸⁴ through a disulfide bond. A single hydrogen bond between the backbone carbonyl of Gly¹⁶⁷ and the backbone amide of Asp¹⁷⁰ was also used to stabilize the 3_{10} -helix within the $\beta 6/\beta 7$ loop, and was substantiated by characteristic NOE patterns from Gly¹⁶⁷-Asp¹⁷⁰. A total of 50 structures were calculated, of which 46 had no NOE, dihedral angle, or scalar coupling violations greater than 0.5 Å, 5°, or 2 Hz, respectively. Of these, 20 structures with the lowest overall energy were chosen to represent the structure of the SrtA-inhibitor complex. The programs MOLMOL^[33] and PYMOL^[34] were used to generate figures.

2.3 | In silico screening of pyridazinone analogues

Ligand preparation, receptor preparation, grid generation, and docking were all conducted with Schrödinger Suite 2011 (Schrödinger LLC, New York, NY, USA). Derivatives of 4-ethoxy-5-mercapto-2-phenylpyridazin-3(2*H*)-one for docking experiments were generated with the CombiGlide application. In CombiGlide, 5-mercapto-2-phenylpyridazin-3(2*H*)-one was defined as the core, and 225, 104, 104, 104, 32, 32, and 22 substituents were created at R2, R3, R4, R5, R6, R7, and R8 sites, respectively (see Figure 4 for definition of the R sites). Substituents were chosen based on the NMR structure of the complex (e.g., polar substituents were added to sites on the inhibitor scaffold that projected into the solvent). The substituents at the R2 site included various polar and non-polar groups of different sizes, as well as a series of substituents with the general formula $-\text{O}(\text{CH}_2)_n\text{X}$, where $n = 1-4$ and X is a polar group. The substituents at R3, R4, and R5 are predominantly polar or positively charged. R6, R7, and R8 contained mostly small hydrophobic substituents. The receptor was processed using the Protein Preparation Wizard, which employs a restrained, partial energy minimization.^[35] The disulfide bond between SrtA and the inhibitor, and the side chain atoms of Cys¹⁸⁷ were removed to prevent steric clashes during docking. Grids were generated by Glide with the grid box set around the inhibitor using default settings. The inhibitor was excluded in the grid calculations. A docking restraint was set up such that the position of the 5-mercapto sulfur atom of the inhibitor derivatives was restricted within 1 Å of the inhibitor sulfur atom in the NMR structure. Docking was carried out with Glide using XP settings.^[36-38] Initially, a total of 623 ligands were docked onto the NMR structure of the protein in the SrtA:inhibitor complex (the co-ordinates of **2-salt** were removed prior to docking). After the first round of docking, the best substituents at each site were selected based on two criteria: 1) their docking score was at least one standard

deviation above the mean docking score of the control compound 4-ethoxy-5-mercapto-2-phenylpyridazin-3(2*H*)-one, and 2) the substituent made a specific interaction with the protein (e.g., a hydrogen bond). This reduced the number of substituents at R2, R3, R4, R5, R6, R7, and R8 to 19, 8, 12, 7, 4, 1 (hydrogen), and 4, respectively. CombiGlide was then used to generate 2,688 compounds with all possible combinations of substituents at R3, R4, R5, R6, and R7, with R2 restricted to ethoxy and R8 restricted to hydrogen. These 2,688 compounds were docked to the NMR structure, and the best substituents were selected as described above. This reduced the number of substituents at R2, R3, R4, R5, R6, R7, and R8 to 19, 3, 3, 1 (hydrogen), 4, 1 (hydrogen), and 4, respectively. CombiGlide was then used again to generate 2,736 compounds with all possible combinations of substituents, and the compounds were again docked to the NMR structure of the protein. Using the same selection criteria, 12, 3, 3, 1 (hydrogen), 4, 1 (hydrogen), and 1 (hydrogen) substituents were chosen at R2, R3, R4, R5, R6, R7, and R8, respectively. Finally, CombiGlide was then used to generate 432 compounds that contained all possible combinations of the substituents.

The top 432 molecules were docked to the enzyme using a procedure that accounts for SrtA mobility. In this procedure, protein motion was first simulated using molecular dynamics (MD) calculations. Bond, angle, and torsion parameters for the inhibitor were derived from the generalized Amber force field (GAFF), using the Antechamber program in Amber.^[39,40] Atomic partial charges were derived from RESP^[41] fitting of Gaussian 09^[42] calculated electrostatic potentials at the Hartree-Fock/6-31G* level. The procedures of MD simulations and clustering were the same as those described in.^[43] Briefly, a 100-ns conventional MD simulation was performed on the SrtA:inhibitor complex using the AMBER99SB-ILDN force field with the simulation package NAMD.^[44,45] Eight hundred frames at regularly spaced intervals were extracted from the last 80 ns of the MD simulation. These frames were aligned by the protein C α atoms in the active site and clustered by root mean square deviation (RMSD) conformational clustering using the GROMOS algorithm as implemented in GROMACS 4.5.^[46] With an RMSD cutoff of 1.40 Å, 25 clusters were obtained, and the centroid member of each cluster was selected to represent each cluster. Subsequently, the top 432 compounds were docked to each of the 25 representative centroid structures, as well as the NMR structure. Procedures used for receptor preparation, grid generation, and docking are the same as those described above. To evaluate the docking results, compounds were ranked by the best docking score they obtained from any of the docking calculations to the NMR or 25 centroid conformers. The top 43 compounds were selected as candidates for synthesis and experimental testing.

2.4 | FRET-based enzymatic assay

The ability of the compounds to inhibit the activity of SrtA was determined using an established Förster resonance energy transfer (FRET) assay.^[19,20] The catalytic domains of SrtA (residues Gln⁶⁰-Lys²⁰⁶) and Ba-SrtA (residues Asp⁵⁷-Lys²¹⁰) were prepared as described previously.^[20,47] Briefly, in the IC₅₀ assay, 20 μl of Sa-SrtA (final assay concentration of 1 μM in FRET buffer: 20 mM HEPES, 5 mM CaCl₂, 0.05% v/v Tween-20, pH 7.5) was incubated with 1 μl of test compound solution (dissolved in 100% DMSO, final assay concentration of 0.08–400 μM) for 1 hr at room temperature. Subsequently, 30 μl of substrate solution, which consists of the self-quenched fluorogenic peptide Abz-LPETG-Dap(Dnp)-NH₂ (32 μM final assay concentration) (Peptide 2.0 Inc., Chantilly, VA, USA) dissolved in FRET buffer, was added to the mixture. Fluorescence was read immediately using an Infinite[®] M1000 PRO (Tecan US Inc., Morrisville, NC, USA) plate reader with the excitation and emission wavelengths set at 335 and 420 nm, respectively. The IC₅₀ assay used to test Ba-SrtA inhibition was similar with the following adjustments: Final assay concentration of Ba-SrtA was 10 μM, final assay concentration of substrate was 100 μM, and the FRET buffer was composed of 20 mM HEPES, 0.05% v/v Tween-20, pH 7.5. IC₅₀ values were calculated by fitting three independent sets of data to Equation 1 using SIGMAPLOT 6.0 (SPSS, Inc., Chicago, IL, USA):

$$\frac{v_i}{v_0} = \frac{1}{1 + \left(\frac{[I]}{IC_{50}}\right)^h} \quad (1)$$

where v_i and v_0 are initial velocity of the reaction in the presence and absence of inhibitor at concentration $[I]$, respectively. The term h is Hill's coefficient.^[48]

For inhibitors that displayed IC₅₀ values lower than half of the enzyme concentration used, data were fit to Morrison's quadratic equation (Equation 2) to calculate the apparent dissociation constant (K_i^{app}):

$$\frac{v_i}{v_0} = 1 - \frac{([E]_T + [I] + K_i^{app}) - \sqrt{([E]_T + [I] + K_i^{app})^2 - 4[E]_T[I]}}{2[E]_T} \quad (2)$$

where v_i and v_0 are initial velocity of the reaction in the presence and absence of inhibitor at concentration $[I]$, respectively. $[E]_T$ is the total active enzyme concentration, and K_i^{app} is the apparent dissociation constant for the enzyme–inhibitor complex.^[48]

To determine the rate of inhibition of SrtA by compounds 2–17, 2–54, and 2–62, the FRET assay we used for IC₅₀ or K_i^{app} determination was modified such that the Abz-LPETG-Dap(Dnp)-NH₂ substrate and inhibitor of various concentrations (final concentration 2.5–14 μM) were added to the

enzyme at the same time. Fluorescence was read every 8 s for a total of 30 min. The reaction progress curve was fit to Equation 3 to determine k_{obs} , the rate constant for conversion from the initial velocity phase to full inhibition:

$$P = \frac{v_i}{k_{obs}} [1 - \exp(-k_{obs}t)] \quad (3)$$

where P is the baseline-corrected fluorescence value, v_i is the initial velocity, and t is time.^[48] These k_{obs} measurements were then plotted against inhibitor concentration and fit to Equation 4 to obtain k_{inact} and K_I values.

$$k_{obs} = \frac{k_{inact}[I]}{K_I + [I]} \quad (4)$$

where k_{obs} is the observed rate constant of inhibition at inhibitor concentration $[I]$, k_{inact} is the maximum rate of inhibition given an infinite concentration of inhibitor, and K_I is the concentration of inhibitor that yields a half-maximum rate of inhibition.^[48]

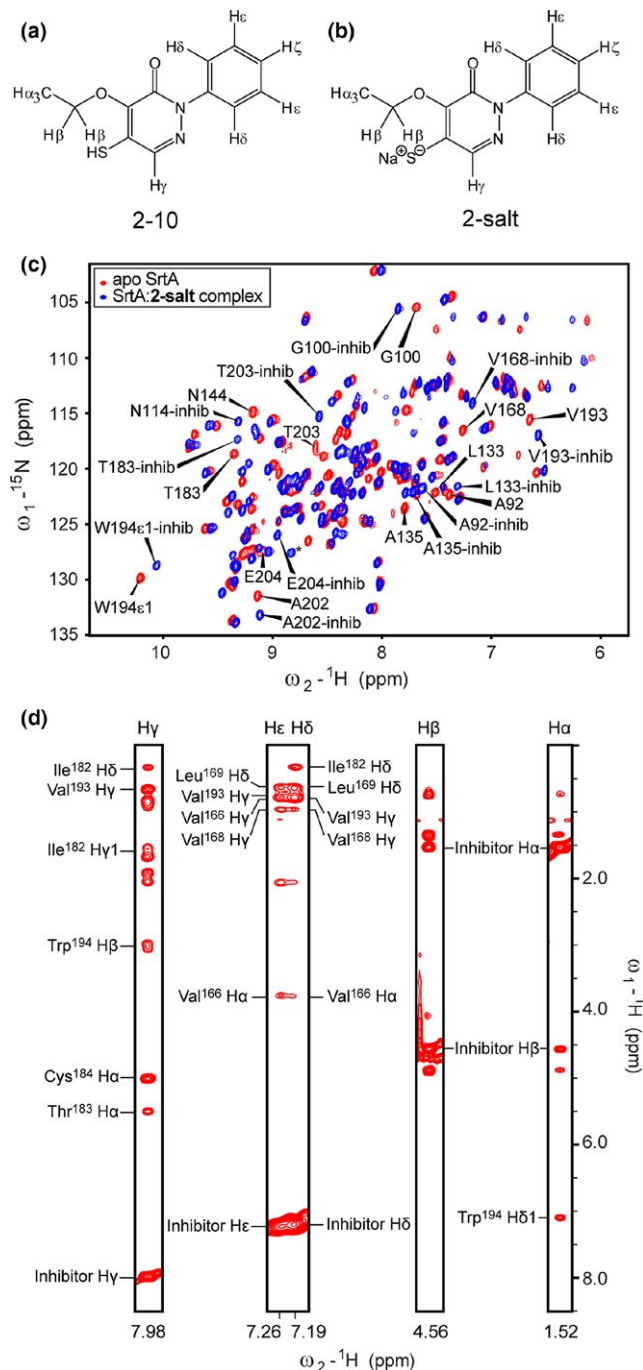
2.5 | Cell wall surface Protein A display assay

Protocol for the cell-based assay was adapted from Zhang *et al.*^[49] Overnight cultures of *S. aureus* were diluted 1:100 into tryptic soy broth (TSB) with or without inhibitor supplement and grown at 37°C with rotation to an A₆₀₀ of 0.5. Molecules 2–62 and 2–17 inhibited bacterial growth at 100 μM, and therefore, these cultures were only diluted back 1:10 into TSB; data are normalized to account for background; 600 μl aliquots were removed, and *S. aureus* were sedimented by centrifugation (12,000×g for 5 min). Bacteria were suspended in 600 μl PBS, 2 μl FITC-labeled IgG (Sigma, St. Louis, MO, USA) was added, and samples were incubated at room temperature for 1 hr. The cells were again sedimented by centrifugation (12,000×g for 5 min) and washed twice with PBS. Bacterial fluorescence intensity was monitored using the Flex Station (Molecular Devices, Sunnyvale, CA, USA) at 495-nm excitation and 520-nm emission. Sample aliquots were spread on TSB agar plates, and CFU were determined to derive relative fluorescence units per A₆₀₀ unit. Triplicate measurements were taken for each trial, and mean and standard deviation were calculated.

2.6 | Cytotoxicity test

The cytotoxicity CC₅₀ of each compound was determined using Promega CellTiter-Glo Luminescent Cell Viability Assay kit (Promega Corp., Madison, WI, USA) by measuring the total ATP levels to quantify the number of metabolically active cells upon drug treatment as described^[50] Briefly, the compounds were diluted in 384 plates (20 μl/well) in

FIGURE 1 NMR spectra of SrtA:**2-salt** complex. (a) Structure of compound **2-10** (4-ethoxy-5-mercapto-2-phenyl-3(2H)-pyridazinone), a previously discovered Sa-SrtA inhibitor with IC_{50} of 13 or 1.5 μM when dimerized through disulfide bond. (b) Structure of the sodium thiolate version of **2-10** (**2-salt**) used in NMR and LC-MS studies. (c) ^1H - ^{15}N HSQC of apo (red) and inhibitor-bound (blue) SrtA after 24 hr of incubation. Peaks that had significant chemical shift changes ($\Delta\delta$) upon binding of the inhibitor are labeled. Significant chemical shift changes are defined as greater than the average $\Delta\delta +$ one standard deviation, where $\Delta\delta = \sqrt{(\Delta\delta_H)^2 + (\Delta\delta_N/6.49)^2}$, and $\Delta\delta_H$ and $\Delta\delta_N$ are the chemical shift changes in Hz for amide proton and amide nitrogen, respectively. (d) Selected panels showing intermolecular NOEs between SrtA and **2-salt**. Identity and chemical shifts for each inhibitor proton are shown at the top and bottom of each panel, respectively. Each assigned cross-peak is labeled with the corresponding proximal SrtA proton. Each assignment was verified in a 3D ^{13}C -edited NOESY by identifying a corresponding inhibitor cross-peak. Not all cross-peaks could be identified due to chemical shift ambiguities, including all NOESY cross-peaks from the inhibitor $\text{H}\beta$ protons



triplicate by a 10-point titration (195 nM to 100 μM) followed by the addition of 30 μl HeLa cells (2500 cells/well). The plates were incubated at 37°C. Three days later, 50 μl of CellTiter-Glo reagent was added to each well followed by a 2-min shaking and a 10-min incubation to lyse the cells. The relative luminescent intensity units (RLU) of each well were measured using an Infinite[®] M1000 PRO (Tecan US Inc., Morrisville, NC, USA) with its green filter and 1 s integration time. CC_{50} values were calculated by fitting the three independent sets of data to Equation 1 using SIGMAPLOT 6.0 (SPSS, Inc., Chicago, IL, USA), by replacing IC_{50} with CC_{50} .

3 | RESULTS

3.1 | NMR structure of SrtA bound to a soluble pyridazinone analogue

Using high-throughput screening methods, we previously discovered that pyridazinone-based molecules effectively inhibit SrtA.^[19] One of the most potent molecules that was discovered was 4-ethoxy-5-mercapto-2-phenylpyridazin-3(2H)-one (hereafter referred as compound **2-10**) (Figure 1a), which inhibits SrtA's *in vitro* activity with an IC_{50} of $13 \pm 1 \mu\text{M}$. However, **2-10** and other pyridazinone-based molecules produced from the screen are poorly soluble in aqueous solvent, and thus could not be optimized using structure-based methods. To overcome this problem, we synthesized a sodium thiolate analogue of **2-10**, 5-ethoxy-6-oxo-1-phenyl-1,6-dihydropyridazine-4-thiolate (**2-salt**) (Figure 1b). **2-salt** exhibits substantially improved solubility (up to 75 mM in aqueous buffer) and inhibits the enzyme with an IC_{50} of $35 \pm 7.4 \mu\text{M}$. Importantly, its increased solubility enables the productive formation of a SrtA:**2-salt** complex

in which the inhibitor is bound to the catalytic domain of sortase (residues Gln⁶⁰-Lys²⁰⁶ of SrtA). The NMR spectra of the complex are well resolved and differ substantially from apo-form of SrtA (Figure 1c). Triple resonance methods were used to assign the protein's ^1H , ^{13}C , and ^{15}N resonances in the SrtA:**2-salt** complex. A comparison with the previously published chemical shift assignments of apo-SrtA reveals large inhibitor-dependent chemical shift changes in atoms that are located within the enzyme's active site, and only small shift changes for atoms located elsewhere in the protein (Figure 1c). A comparison of the NOESY spectra of the complex and apo-SrtA reveals that residues located distal

to the active site exhibit similar NOE cross-peak patterns. We conclude from these data that the inhibitor binds to the enzyme's active site where it causes only localized structural changes.

NMR spectroscopy was used to define the structure of the SrtA:2-salt complex. Near-complete chemical shift assignments were obtained for both the protein and bound inhibitor. Because the inhibitor causes only localized changes in the structure of the enzyme, we employed a hybrid approach to determine the structure of the complex. NMR data were used to define the molecular basis of inhibitor binding in the SrtA:2-salt complex (see Section 2). A total of 229 experimental restraints define the structure of the enzyme's active site, including 156 intramolecular protein-protein distance, 20 intermolecular inhibitor-protein NOE distance, 43 ϕ and ψ dihedral angle, and 10 $^3J_{\text{HN-H}\alpha}$ coupling constant restraints. An ensemble containing 20 conformers representing the structure of the complex exhibit good covalent geometries and have no NOE, dihedral angle, or scalar coupling violations greater than 0.5 Å, 5°, or 2 Hz, respectively. Enzyme interactions with the inhibitor are well defined by

the NMR data, as the co-ordinates of the backbone and heavy atoms within the active site, as well as the inhibitor molecule have a root mean square deviation (RMSD) to the mean structure of 0.20 ± 0.07 and 0.69 ± 0.06 Å, respectively. Complete structure and restraint statistics are presented in Table 1.

The structure of the complex reveals that the pyridazinone inhibitor binds to a groove adjacent to the enzyme's active site (Figure 2a–d). The base of the group was formed by residues in strands $\beta 4$ and $\beta 7$, while residues located in the $\beta 2/\text{H}1$, $\beta 3/\beta 4$, $\beta 6/\beta 7$, and $\beta 7/\beta 8$ loops form the sides of the groove and partially shield the inhibitor from solvent. Numerous hydrophobic contacts are made to the 2-phenyl group of the inhibitor from the side chains of Val¹⁶⁶, Val¹⁶⁸, and Leu¹⁶⁹ within the $\beta 6/\beta 7$ loop, Val¹⁹³ within the $\beta 7/\beta 8$ loop, and Ile¹⁸² on strand $\beta 6$ (Figure 2c). These interactions are supported by intermolecular NOEs between the Val¹⁶⁶ H α , Val¹⁶⁶ H γ , Val¹⁶⁸ H γ , Leu¹⁶⁹ H δ , and Val¹⁹³ H γ protons of the enzyme, and the H ϵ and H δ protons of the inhibitor (Figure 1d). Interestingly, an NOE was identified between the H δ proton of Ile¹⁸² and the H δ proton of the inhibitor,

TABLE 1 Statistics for the NMR modeled structure of SrtA bound to a pyridazinone inhibitor 2-salt

	SA ^a	$\overline{\text{SA}}$ ^a
RMS deviations from NOE interproton distance restraints (Å)		
Intramolecular ^b (156)	0.075 ± 0.003	0.087
Intermolecular (20)	0.104 ± 0.007	0.121
RMS deviations from dihedral angle restraints (°) ^c (43)		
	0.824 ± 0.068	0.715
RMS deviations from $^3J_{\text{HN}}^{\alpha}$ coupling constants (Hz) ^c (10)		
	0.451 ± 0.027	0.772
Deviations from idealized covalent geometry		
Bonds (Å)	0.0040 ± 0.0000	0.00574
Angles (°)	1.048 ± 0.002	1.0697
Improper (°)	1.545 ± 0.026	1.5550
PROCHECK-NMR ^d		
Most favorable region (%)	66.5 ± 2.9	66.7
Additionally allowed region (%)	29.3 ± 3.2	28.6
Generously allowed region (%)	4.3 ± 1.5	4.8
Disallowed region (%)	0.0 ± 0.0	0
Co-ordinate precision ^e		
Protein backbone (Å)	0.20 ± 0.07	
Protein heavy atoms (Å)	0.69 ± 0.06	

^aThe notation of the NMR structures is as follows: SA represent an ensemble of 20 best structures calculated by simulated annealing. $\overline{\text{SA}}$ is the average energy-minimized structure. The number of terms for each restraint is given in parentheses. None of the structures exhibited distance violations greater than 0.5 Å, dihedral angle violations greater than 5°, or coupling constant violations greater than 2 Hz.

^bIntramolecular NOE distance restraints include any NOE signals from any residue in the Sa-SrtA enzyme to residues Val¹⁶⁶-Lys¹⁷⁵, Thr¹⁸³-Lys¹⁹⁶, and the side chains from residues Leu⁹⁷, Ser¹¹⁶, His¹²⁰, Thr¹⁸⁰, Ile¹⁸², Arg¹⁹⁷, Ile¹⁹⁹, and Val²⁰¹.

^cExperimental backbone dihedral angle restraints comprised 21 ϕ and 22 ψ angles within residues Val¹⁶⁶-Lys¹⁷⁵ and Thr¹⁸³-Lys¹⁹⁶.

^dPROCHECK-NMR data includes residues Val¹⁶⁶-Lys¹⁷⁵ and Thr¹⁸³-Lys¹⁹⁶ of the Sa-SrtA:inhibitor complex.

^eThe co-ordinate precision is defined as the average atomic RMS deviation of the 20 individual simulated annealing structures and their mean co-ordinates. The reported values are for residues Val¹⁶⁶-Lys¹⁷⁵ and Thr¹⁸³-Lys¹⁹⁶ of the Sa-SrtA:inhibitor complex for the protein backbone RMS deviation. In addition, residues Leu⁹⁷, Ser¹¹⁶, His¹²⁰, Thr¹⁸⁰, Ile¹⁸², Arg¹⁹⁷, Ile¹⁹⁹, and Val²⁰¹ were included for calculating protein heavy atom RMS deviation.

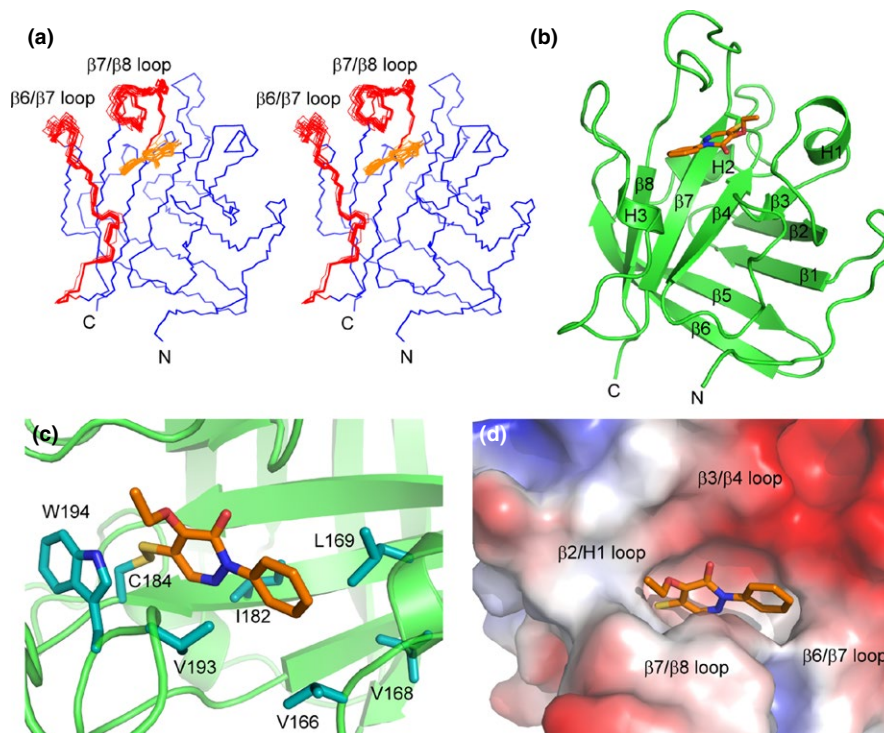


FIGURE 2 NMR solution structure of the SrtA:2-salt complex. (a) Cross-eyed stereo image showing the ensemble of 20 lowest energy structures of the SrtA:2-salt complex. The bound compound **2-salt** is shown in orange, and protein backbone atoms allowed to move during molecular dynamics simulations are shown in red (Val¹⁶¹-Lys¹⁷⁵ and Thr¹⁸³-Lys¹⁹⁶). The bundle is aligned using all of the protein backbone heavy atoms and the heavy atoms from the inhibitor. (b) Ribbon structure of the SrtA:2-salt complex. The covalently bound inhibitor is shown in stick representation and colored orange. (c) Expanded view of the SrtA active site with the inhibitor bound. Side chains of residues exhibiting intermolecular NOEs to the inhibitor are shown in cyan sticks. A hydrophobic pocket formed by Val¹⁶⁶, Val¹⁶⁸, Leu¹⁶⁹, and Ile¹⁸² bind the 2-phenyl group of the inhibitor, while the remainder of the inhibitor is positioned over the $\beta 7$ and $\beta 8$ strands. (d) Expanded view of the SrtA active site with the protein represented by its solvent accessible surface. The surface is colored by its electrostatic properties from acidic (red) to basic (blue)

whereas no NOEs were observed to the inhibitor's He proton. This is consistent with the structure complex, as the 2-phenyl group is only partially buried within a hydrophobic pocket; it is sandwiched between the side chains of Val¹⁹³ on the $\beta 7/\beta 8$ loop and Leu¹⁶⁹ on the $\beta 6/\beta 7$ loop. The positioning of the central pyridazinone ring of the inhibitor is also well defined by the NMR data as NOEs between its H γ atom and the Thr¹⁸³ H α (strand $\beta 7$), Cys¹⁸⁴ H α (strand $\beta 7$), Trp¹⁹⁴ H β ($\beta 7/\beta 8$ loop), Ile¹⁸² H $\gamma 1$ (strand $\beta 7$), Ile¹⁸² H δ (strand $\beta 7$), and Val¹⁹³ H γ ($\beta 7/\beta 8$ loop) protons are observed (Figure 1d). This orients the central ring such that the carbonyl group is directed toward the solvent, while the H γ atom faces strand $\beta 7$. The indole ring of Trp¹⁹⁴ on the $\beta 7/\beta 8$ loop closes the inhibitor recognition groove, shielding the disulfide bond between the inhibitor and Cys¹⁸⁴ from the solvent. This is evidenced by NOEs between the He1, H $\zeta 2$, and H $\zeta 3$ atoms of the indole ring of Trp¹⁹⁴, and the H δ methyl protons on Leu⁹⁷ within helix H1. This demonstrates the $\beta 7/\beta 8$ loop of the **2-salt** bound enzyme is positioned in a manner more similar to the apo-SrtA enzyme with the loop pressed against H1, and differs from the substrate-bound

form of the enzyme, as these elements are separated by ~ 13 Å (see Section 4).^[20,32] The precise location of 4-ethoxy moiety is not well defined by the NMR data, as only a single NOE defines its positioning (between Trp¹⁹⁴ H $\delta 1$ and H α methyl of the inhibitor). However, in nearly all conformers within the ensemble it is positioned within a narrow groove formed between the $\beta 7/\beta 8$ and $\beta 2/H1$ loops.

In the structure of the complex, the sulphhydryl group of the active site cysteine residue (Cys¹⁸⁴) is positioned adjacent to the 5-mercapto group of the inhibitor, suggesting that they may be joined via a disulfide bond. Although the mechanism of inhibition by the pyridazinone-based compounds is not known, the most potent pyridazinone molecules also contain 5-mercapto group consistent with them also covalently modifying the enzyme. To determine the mechanism of inhibition, we incubated 10-fold molar excess of **2-salt** with SrtA, unbound **2-salt** was then removed by dialysis and the **2-salt**:SrtA complex was digested with trypsin. The digestion products were then analyzed using LC-MS before and after adding DTT. In the absence of DTT, a peak eluting at 6.86 min has a mass-to-charge ratio consistent

with it being a disulfide-linked QLTLITCDDYNEK:**2-salt** peptide, compatible with cysteine modification (Figure 3a,b). Moreover, when DTT is added this complex disappears and a new peak corresponding to the unmodified QLTLITCDDYNEK elutes at 5.09 min (Figure 3a,c). Similar LC-MS results were obtained when the parent compound **2-10** was reacted with the enzyme (data not shown). These data indicate pyridazinone-containing inhibitors such as **2-salt** and **2-10** inactivate SrtA by forming disulfide bond to Cys¹⁸⁴.

3.2 | Structure-based inhibitor optimization

Using the atomic co-ordinates of the SrtA:**2-salt** complex, computational approaches were used to quantitatively predict

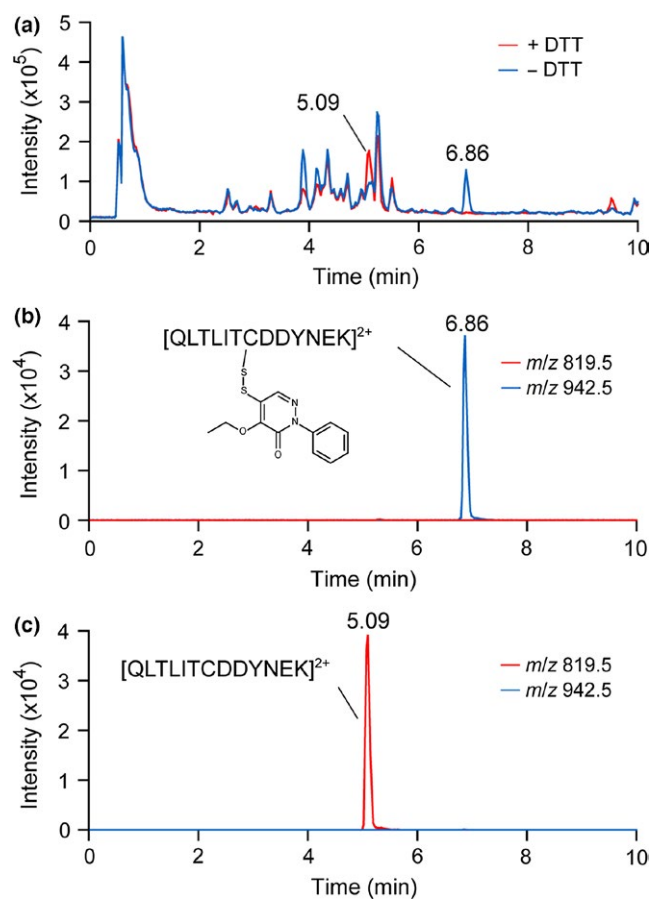


FIGURE 3 LC-MS traces of the SrtA:**2-salt** complex. (a) Overlay of the total ion traces of trypsin-digested 1:1 mixture of SrtA and **2-salt** before (blue) and after (red) addition of 5 mM DTT. Major differences occur at retention times 5.09 min and 6.86 min. (b) Chromatogram of trypsin-digested sample without addition of DTT. Only the traces of ions with m/z of 819.5 (red) and 942.5 (blue) are shown, which correspond to the $[M + 2H]^{2+}$ ions of the unmodified Cys¹⁸⁴-containing peptide and **2-salt** modified version of the peptide, respectively. (c) Similar to (b), but the chromatogram shown is the trypsin-digested sample with the addition of DTT

inhibitor modifications that could increase binding affinity and selectivity. In this procedure, analogues of the **2-10** pyridazinone compound were constructed in silico using the program CombiGlide and their binding poses and energies evaluated using the molecular docking program Glide. Briefly, the 5-mercapto-2-phenylpyridazin-3(2*H*)-one moiety of **2-10** was defined as the core in CombiGlide, and substituents derived from the program's fragment library were then systematically added to eight sites (Figure 4, sites named R2 to R8). The substituents were chosen based on their degree of solvent exposure, and for buried substituents, the accessible volume available to them within the enzyme's subsite. In particular, sites on the small molecule that are solvent exposed (R2–R5) were modeled with predominantly polar groups of various sizes, while sites located on the protein-facing side of the molecule (R6–R8) were modeled to contain mostly small hydrophobic groups (see Section 2). Initially, 6,047 analogues of **2-10** were computationally evaluated, which included 623 analogues containing a single alteration, and 5,424 analogues containing two alterations at sites R2 to R8 (Figure 4). Each analogue was then docked to the NMR structure and ranked based on their docking score. Analogues containing single-site modifications at R2, R3, R4, and R6 exhibited the largest

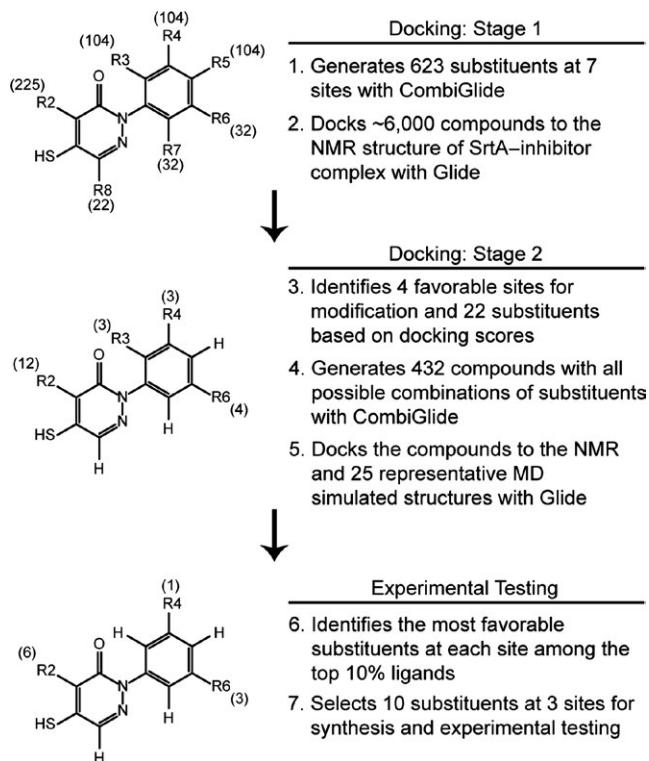


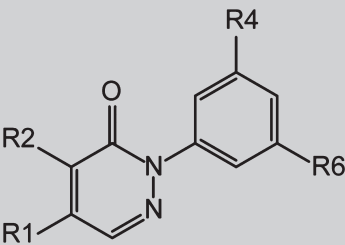
FIGURE 4 Overview of the molecular docking and experimental testing process. Description of the docking, substituent selection, and experimental testing processes are shown on the right. The structure of the core of the pyridazinone compound is shown on the left. The number of substituents at each site is indicated in parentheses

improvements in binding (12, 3, 3, and 4 analogues containing unique substituents at these sites resulted in improved binding, respectively). Next, to discover small molecules with even greater binding affinity, docking experiments were performed for 432 analogues that each contained four alterations. The small molecules contained substituent changes at their R2, R3, R4, and R6 sites, which were chosen based on the aforementioned single-site docking studies. During this phase of the work, the docking calculations made use of the relaxed complex scheme approach to account for protein flexibility in the enzymes active site as previously described.^[43,51,52] After completing the computational docking experiment, a total of 43 compounds were analyzed further, as their docking scores ranked in top 10% of the 432 analogues that were tested. These “top” molecules had docking scores ranging from -8.9 to -10.0, which is a significant improvement as compared to the **2-10** lead molecule (-4.08). An inspection of their chemical structures reveals that modification at sites R2, R4, and R6 are most beneficial (R2, $-\text{O}(\text{CH}_2)_2\text{OH}$, $-\text{O}(\text{CH}_2)_3\text{OH}$, $-\text{OCH}_2\text{COOH}$, $-\text{O}(\text{CH}_2)_2\text{COOH}$, $-\text{OCH}_2\text{CONH}_2$, and $-\text{O}(\text{CH}_2)_2\text{CONH}_2$;

R4, $-\text{C}(=\text{NH})\text{NH}_2$ (hereafter referred as amidine); R6, $-\text{CH}_3$, $-\text{F}$, and $-\text{OCH}_3$).

Several promising pyridazinone analogues based on the docking analysis were synthesized and their inhibitory activity determined experimentally using a FRET-based assay (Table 2). Representative dose-response curves are shown in Fig. S1. Analogues were chosen for further study based on their synthetic feasibility and in order to maximize the chemical diversity of the molecular scaffolds that were tested. Initially, ten analogues of **2-10** were synthesized that contained single-site changes (**2-51** to **2-60**). As **2-10** oxidizes readily to form a more potent and stable symmetric disulfide dimer (**2-17**), all of the analogues were tested in their oxidized form and their potency compared to **2-17**. Improvements of twofold to 10-fold were obtained by making single-site alterations. In particular, non-polar modifications at site R6 are beneficial, presumably increasing van der Waals contacts to residues in the $\beta 6/\beta 7$ loop of the enzyme that form a hydrophobic pocket (Figure 2c,d). In agreement with the structure, the R4 site on the opposite side of the benzene

TABLE 2 SrtA inhibition of the pyridazinone compound derivatives



Compound	R1	R2	R4	R6	Sa-SrtA IC ₅₀ (μM) ^a	Ba-SrtA IC ₅₀ (μM) ^b	CC ₅₀ (μM)	cLogP
2-10	SH	OCH ₂ CH ₃	H	H	13 ± 1 ^d	3.2 ± 1.7 ^d	n.d. ^e	3.03
2-17	S-SR ^c	OCH ₂ CH ₃	H	H	1.5 ± 0.4 ^d	1.2 ± 0.4 ^d	~100	4.37
2-51	S-SR ^c	OCH ₂ CH ₃	H	F	0.16 ± 0.04	1.34 ± 0.62	~100	4.55
2-52	S-SR ^c	OCH ₂ CH ₃	H	CH ₃	1.40 ± 0.30	0.49 ± 0.11	n.d. ^e	4.58
2-53	S-SR ^c	OCH ₂ CH ₃	H	OCH ₃	0.62 ± 0.18	0.15 ± 0.05	~100	4.46
2-54	S-SR ^c	OCH ₂ CH ₃	C(=NH)NH ₂	H	0.54 ± 0.14	2.08 ± 0.55	>100	2.72
2-55	S-SR ^c	O(CH ₂) ₂ OH	H	H	0.22 ± 0.04	0.33 ± 0.14	>100	2.35
2-56	S-SR ^c	O(CH ₂) ₃ OH	H	H	0.84 ± 0.06	1.86 ± 0.59	~100	2.80
2-57	S-SR ^c	OCH ₂ COOH	H	H	2.20 ± 0.20	0.49 ± 0.19	n.d. ^e	2.02
2-58	S-SR ^c	O(CH ₂) ₂ COOH	H	H	6.10 ± 0.50	9.98 ± 0.37	>100	2.32
2-59	S-SR ^c	OCH ₂ CONH ₂	H	H	22 ± 2	94 ± 23	n.d. ^e	2.11
2-60	S-SR ^c	O(CH ₂) ₂ CONH ₂	H	H	3.25 ± 0.34	11.90 ± 0.70	>100	2.06
2-61	S-SR ^c	O(CH ₂) ₂ OH	H	F	0.41 ± 0.12	0.60 ± 0.23	>100	2.83
2-62	S-SR ^c	O(CH ₂) ₃ OH	H	F	0.02 ± 0.01	0.45 ± 0.29	~100	3.43

^aOr K_i^{app} for values that are lower than 0.5 μM as determined by Morrison's equation.

^bOr K_i^{app} for values that are lower than 5 μM as determined by Morrison's equation.

^cS-SR indicates that the compound is a disulfide-bonded dimer.

^dValues taken from reference.¹⁹

^en.d., no data.

ring is also a good site for the addition of a polar amidine group, which presumably enables contacts to Glu¹⁰⁵ located in the β 3/ β 4 loop. Altering the length and polar character of the substituent attached to the R2 site is also advantageous, presumably because it enables the formation of additional hydrogen bonds to the residues located within the β 7/ β 8 loop (e.g., Tyr¹⁸⁷, Gly¹⁹², and Trp¹⁹⁴). Two analogues, **2-61** and **2-62**, were synthesized that simultaneously alter substituents at sites R2 and R6. Compound **2-61** combines favorable O(CH₂)₂OH (R2) and F (R6) modifications, but surprisingly did not show a substantial improvement in activity. In contrast, significant improvements in activity are observed in compound **2-62** that combines O(CH₂)₃OH (R2) and F (R6) alterations (IC₅₀ value of 0.02 ± 0.01 μ M). A more complete description of the structure–activity relationship analysis is provided in Section 4.

In order to determine whether the compounds had broad-spectrum activity against sortase enzymes, we tested their ability to inhibit the *Bacillus anthracis* class A sortase enzyme (Ba-SrtA), which similar to *S. aureus* SrtA (Sa-SrtA) anchors proteins to the cell wall that contain an LPXTG sorting signal. In general, all of the analogues had good inhibitory activity against Ba-SrtA, with IC₅₀ values in the low micromolar to high nanomolar range. However, distinct species-specific trends in inhibitory activity are apparent. For example, the most effective SrtA inhibitor (**2-62**) is 20-fold less active against Ba-SrtA (IC₅₀ = 0.45 ± 0.29 μ M against Ba-SrtA as compared to IC₅₀ = 0.02 ± 0.01 μ M against Sa-SrtA), whereas the best Ba-SrtA inhibitor compound **2-53** containing a methoxy group at the R3 site is fourfold more active against Ba-SrtA as compared to SrtA (Ba-SrtA IC₅₀ = 0.15 ± 0.05 μ M versus Sa-SrtA IC₅₀ = 0.62 ± 0.18 μ M). These subtle differences in potency likely arise from structural differences between the active sites of each enzyme, but nevertheless indicate that pyridazinone-based inhibitors are capable of inhibiting class A type sortases that recognize LPXTG sorting signals.

3.3 | Inhibitor inactivation kinetics and effect on protein display in intact cells

For the parent compound (**2-17**), positively charged compound (**2-54**), and the most potent compound based on its IC₅₀ value (**2-62**), we determined the rate at which they inactivate SrtA. The substrate and inhibitor were simultaneously added to SrtA and the observed rate constant of inhibition (k_{obs}) was determined by fitting the progress curve to Equation 3 (see Section 2). Measurement of k_{obs} at different inhibitor concentrations yields k_{inact} , the rate constant describing inhibitor covalent modification of the enzyme, and K_I , which carries the same intrinsic kinetic significance as K_m and approximates the dissociation constant of the non-covalent E–I complex. The overall inactivation efficiency is a function

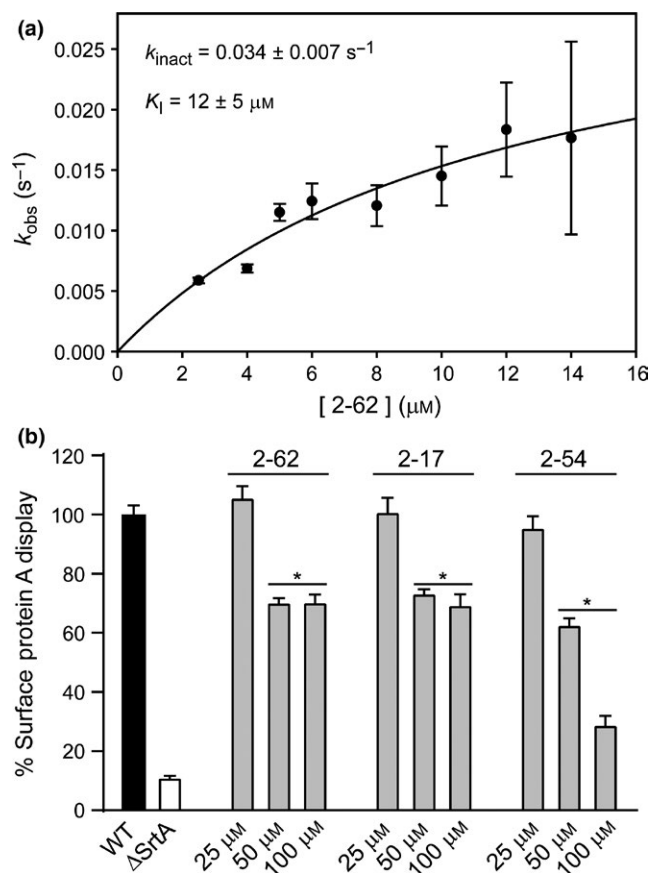


FIGURE 5 Inhibitor inactivation kinetics and effect on protein display. (a) The rate of SrtA inhibition by compound **2-62** was determined by calculating k_{obs} for each inhibitor concentration using Equation 3 and subsequently calculating k_{inact} and K_I using Equation 4 listed in Section 2. This graph shows a representative curve of fitting the k_{obs} data with Equation 4. (b) The abundance of surface protein A displayed on *S. aureus* cell wall in the absence (control) or presence of pyridazinone inhibitor was quantified with a FITC-labeled IgG binding assay. Statistical significance (* $p < .0007$) was determined using the unpaired, two-tailed Student's t test ($n = 3$, shown with standard deviation)

TABLE 3 Inactivation kinetics of pyridazinone compound derivatives

Compound	k_{inact} (s ⁻¹)	K_I (μ M)	k_{inact}/K_I ($\mu\text{M}^{-1}\text{s}^{-1}$)
2-17	0.004 ± 0.001	5 ± 3	0.0008 ± 0.0005
2-54	0.015 ± 0.003	24 ± 9	0.0006 ± 0.0003
2-62	0.034 ± 0.007	12 ± 5	0.003 ± 0.001

of covalent modification rate and binding affinity (k_{inact}/K_I). Figure 5a shows a representative plot of k_{obs} measured as a function of inhibitor (**2-62**) concentration, which yields k_{inact} of 0.034 ± 0.007 s⁻¹, K_I of 12 ± 5 μ M and k_{inact}/K_I of 0.003 ± 0.001 $\mu\text{M}^{-1}\text{s}^{-1}$. Complete results are summarized in Table 3. Consistent with the IC₅₀ results, inactivation efficiency is significantly higher for **2-62** (0.003 ± 0.001 $\mu\text{M}^{-1}\text{s}^{-1}$),

as compared to **2-54** ($0.0006 \pm 0.0003 \mu\text{M}^{-1}\text{s}^{-1}$) or **2-17** ($0.0008 \pm 0.0005 \mu\text{M}^{-1}\text{s}^{-1}$).

The ability of the most promising inhibitors to disrupt sortase-mediated protein display in intact *S. aureus* cells was determined. In Newman strain of *S. aureus*, SrtA anchors 19 different surface proteins in the bacterial envelope,^[53] including SpA, a molecule that binds the Fc γ and Fab domains of host immunoglobulins.^[54] The abundance of Ig binding to SpA in the bacterial cell wall envelope is therefore dependent upon the activity of *S. aureus* SrtA, enabling the effects of the pyridazinone molecules on SpA display to be measured. In the assay, cells are cultured with varying amounts of inhibitor and the amount of displayed SpA then quantified by adding fluorescein isothiocyanate (FITC)-labeled IgG. As expected, a Δ srtA control strain displays significantly less SpA on its surface; protein display is reduced by ~80% in Δ srtA as compared to WT *S. aureus* (Figure 5b). The addition of compounds **2-17**, **2-54**, or **2-62** to WT *S. aureus* cultures caused statistically significant reductions in SpA display. The largest effects are observed when **2-54** is added, which shows a dose-dependent decrease in SpA display. When 100 μM is present in the cell culture, display levels are reduced to 35% of WT, approaching levels observed for the Δ srtA strain.

To gain insight into the therapeutic window at which the pyridazinone inhibitors could be dosed to treat *S. aureus* infections, their cytotoxicity against human cells was determined. In general, all of the compounds tested exhibit minimal cytotoxicity against human HeLa cells, as they have CC₅₀ values in excess of 100 μM (Table 2). Notably, the most potent inhibitor, **2-62**, has a CC₅₀ to IC₅₀ ratio as large as 5,000. Interestingly, an analysis of the data reveals that the CC₅₀ values of the compounds are inversely correlated to their predicted octanol–water partition coefficients (cLogP), with molecules that have smaller (more negative) cLogP values exhibiting some of the highest CC₅₀ values. This is not surprising, as a more negative cLogP value indicates that a compound is more soluble in water, and therefore less likely to be capable of crossing the cellular membrane where it could cause off-target effects that lead to cell death. As SrtA is located on the extracellular membrane of *S. aureus*, additional modification of the pyridazinone analogues to increase their solubility in water may further reduce off-target cellular toxicity.

4 | DISCUSSION

The emergence of methicillin-resistant *S. aureus* (MRSA) and other multidrug-resistant bacterial pathogens has created an urgent need for new antibiotics. The *S. aureus* SrtA enzyme is an attractive drug target as it covalently attaches virulence factors to the microbial surface that have important functions in the infection process, including mediating

bacterial adhesion to host tissues, nutrient acquisition, and the suppression and evasion of the immune system. SrtA's importance has been validated in animal models of infection that demonstrate that *S. aureus* srtA⁻ mutants have attenuated virulence. To date, several synthetic, peptide-based, and natural product inhibitors of SrtA have been reported,^[55] but only a few investigators have been able to rationally optimize these molecules using structural biology approaches. This is because it has been problematic to study the enzyme using X-ray crystallography, as its active site exhibits a high degree of conformational disorder that hinders crystallization. Moreover, the conformational disorder makes accurate computational modeling of enzyme–inhibitor interactions challenging. To overcome these problems, we employed a novel soluble pyridazinone analogue that enabled the NMR structure of enzyme pyridazinone to be determined. Using the structure of the complex, we rationally optimized several pyridazinone-based inhibitors of SrtA, leading to new second-generation molecules that have improved inhibitory activity and lower cellular toxicity.

Our structural studies of the water soluble pyridazinone inhibitor, **2-salt**, reveal that it causes a disordered to ordered structural change in the enzyme's active site that is reminiscent of the previously documented changes caused by binding the sorting signal substrate. Our previous NMR studies of SrtA in its apo-state have revealed that it contains a large active site loop that connects strands β 6 to β 7 (the β 6/ β 7 loop). In the absence of the substrate, the loop is structurally disordered and undergoes motions on the micro- to millisecond timescale.^[20] However, upon binding the LPXTG sorting signal, motions in the loop are quenched, as a result of a disordered to ordered conformational change that enables it to partially encapsulate the leucine side chain within the bound peptide.^[32] Interestingly, in the structure of the SrtA:**2-salt** complex, the inhibitor binds to the same site on SrtA as the LPXTG sorting signal, and similar to the substrate, it alters the structure and dynamics of the β 6/ β 7 active site loop (Figure 6). In the SrtA-sorting signal substrate complex, residues Val¹⁶⁶-Leu¹⁶⁹ the β 6/ β 7 loop form a 3_{10} -helix that facilitates closure over the substrate by forming a non-polar surface that contacts the leucine side chain. In the SrtA:**2-salt** complex, the 2-phenyl group in the inhibitor mimics the leucyl side chain, as contacts to it drive loop closure and formation of a 3_{10} -helix. However, as compared to the substrate complex, the residues in the newly formed 3_{10} -helix are shifted by one amino acid in the primary sequence; in the SrtA:**2-salt** and SrtA–substrate complexes, the newly formed active site helix is comprised of residues Gly¹⁶⁷-Asp¹⁷⁰ and residues Val¹⁶⁶-Leu¹⁶⁹, respectively. This subtle shift is presumably caused by inhibitor contacts originating from side chains of Val¹⁶⁶ and Leu¹⁶⁹, which in the SrtA:**2-salt** complex pack against the 2-phenyl group of the inhibitor necessitating that the backbone atoms of Val¹⁶⁶ adopt an extended

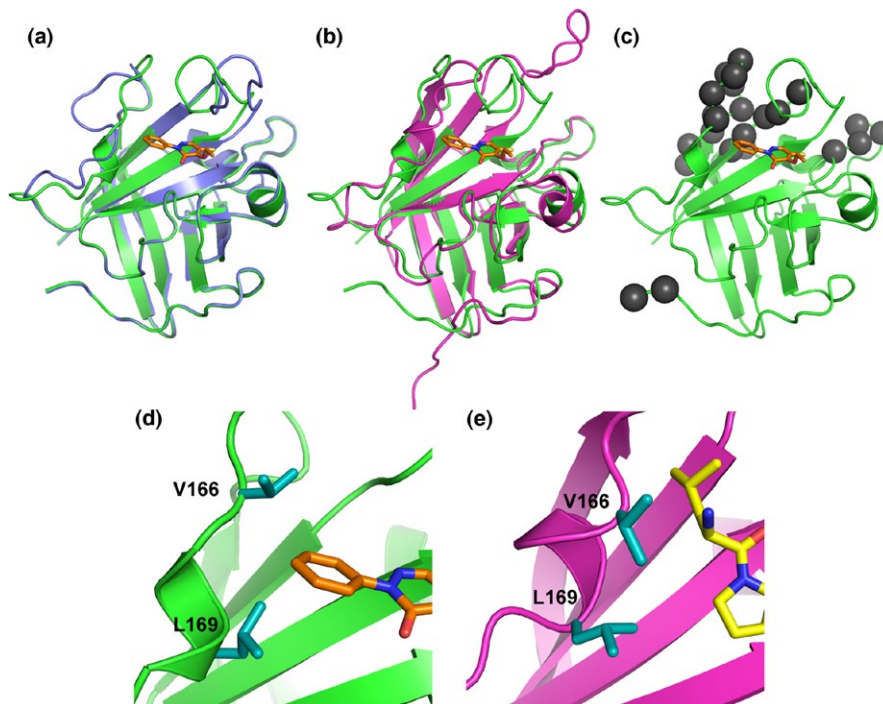


FIGURE 6 Comparison of the SrtA:2-salt structure with apo- and holo-SrtA structures. SrtA:2-salt complex (green) superimposed with (a) apo-SrtA (blue, PDB code 1IJA) and (b) SrtA:LPAT* complex with the substrate analogue LPAT* removed (pink, PDB code 2KID). In apo-SrtA, residues Ser¹⁵⁷-Lys¹⁷⁵ are unstructured in the $\beta 6/\beta 7$ loop. In inhibitor complex, a portion of this loop is immobilized. The $\beta 6/\beta 7$ loop in the SrtA:2-salt complex is unstructured from residues Thr¹⁵⁶-Asp¹⁶⁵, similar to apo-SrtA, and adopts a single conformation from residues Val¹⁶⁶-Lys¹⁷⁵, as seen in the SrtA:LPAT* structure. The $\beta 7/\beta 8$ loop adopts a conformation more closely resembling the apo-SrtA structure. (c) Non-proline amide cross-peaks that were not detected in the ¹H-¹⁵N HSQC spectra are shown in gray spheres. These residues include Met⁵⁹-Gln⁶⁰, Thr¹²¹-Asp¹²⁴, Lys¹³⁷, Thr¹⁵⁶-Val¹⁶⁶, and Lys¹⁹⁶-Phe²⁰⁰. (d) Expanded view of the $\beta 6/\beta 7$ loop 3_{10} -helix in the SrtA:2-salt complex with 2-salt represented as orange sticks. (e), expanded view of the $\beta 6/\beta 7$ loop and 3_{10} -helix in the SrtA:LPAT* complex with LPAT* represented as yellow sticks

conformation (Figure 6d). In contrast, in the SrtA:substrate complex, Val¹⁶⁶ adopts a helical conformation such that its side chain is rotated away from the active site so as to accommodate the leucine side chain of the sorting signal substrate (Figure 6e).

The pyridazinone inhibitor does not fully mimic the sorting signal substrate as its binding only partially closes the $\beta 6/\beta 7$ loop and it fails to substantially reposition the $\beta 7/\beta 8$ loop active site loop. In our previously reported structure of the SrtA-substrate complex, in addition to inducing a 3_{10} -helix formation within the $\beta 6/\beta 7$ loop, substrate binding also caused a disordered to ordered transition in residues that immediately preceded the helix in the primary sequence. These changes fully closed the loop, and presumably constructed a catalytically competent active site in which the side chain guanidino group of Arg¹⁹⁷ is positioned to stabilize high-energy anionic reaction intermediates. However, in the structure of the inhibitor complex, the active site does not fully form as this region of the $\beta 6/\beta 7$ loop remains flexible and disordered. This is evidenced by the absence of NMR resonances for residues Thr¹⁵⁶-Asp¹⁶⁵ in the $\beta 6/\beta 7$ loop in both the apo- and inhibitor-bound forms of the enzyme, which are

presumably broadened beyond detection because of motions on micro- to millisecond timescale (Figure 6c). This notion is also substantiated by the absence of signals for residues Arg¹⁹⁷-Phe²⁰⁰ in strand $\beta 8$ in both forms of the enzyme, which are presumably rigid, but broadened beyond detection because their magnetic environments fluctuate as a result of motions in the proximal $\beta 6/\beta 7$ loop. A comparison of the substrate- and inhibitor-bound forms of the enzyme also reveals other key differences. Previously, we have shown that upon binding the signal analogue the $\beta 7/\beta 8$ loop in SrtA is displaced by ~ 13 Å. This rearrangement results in the formation of a new groove between the $\beta 7/\beta 8$ loop and helix H1, which has been hypothesized to form the binding site of the secondary substrate, the Gly₅ cross-bridge of lipid II. Interestingly, binding of the inhibitor displaces the loop by only ~ 3.5 Å, such that the groove is not exposed. This is substantiated by the presence of NOEs in the spectra of the inhibitor complex between H ϵ 1, H ζ 2, and H ζ 3 of the indole ring of Trp¹⁹⁴ located in the $\beta 7/\beta 8$ loop and H δ methyl protons on Leu⁹⁷ within helix H1 (similar NOEs are present in the NMR spectra of the apo-form of the enzyme, but absent in the SrtA-substrate complex). Thus, although the inhibitor

triggers partial closure of the $\beta 6/\beta 7$ loop and the 3_{10} -helix formation similar to the sorting signal substrate, the changes are less substantial and the conformation and dynamics of residues in the $\beta 6/\beta 7$ loop nearest the active site, as well as the $\beta 7/\beta 8$ loop, are not significantly affected by inhibitor binding.

The structure of the SrtA:**2-salt** complex is the first high-resolution structure of a SrtA-type enzyme bound to a small-molecule inhibitor. Previously, Zhulenkova and colleagues solved the NMR structure of *S. aureus* SrtA in complex with a benzisothiazolinone-based inhibitor.^[16] However, the coordinates of the inhibitor were not well defined, as only nine intermolecular enzyme–inhibitor NOEs defined its positioning. The authors speculated that both the $\beta 6/\beta 7$ and $\beta 7/\beta 8$ loops in the SrtA–benzisothiazolinone complex are partially disordered such that the bound inhibitor can adopt different conformations. This is distinct from pyridazinone-based molecules, as in the SrtA:**2-salt** complex a portion of the $\beta 6/\beta 7$ loop near the inhibitor becomes structurally ordered and the $\beta 7/\beta 8$ loop is structurally ordered and adopts a closed conformation that is similar to its conformation in the apo-form of the protein. Nevertheless, their binding mechanisms share two common features. First, both pyridazinone and benzisothiazolinone inhibitors covalently modify SrtA by forming a disulfide bond with Cys¹⁸⁴. Second, despite the flexibility of the benzisothiazolinone compound and the partially disordered active site loops, in both inhibitor complexes the side chains of Val¹⁶⁶, Val¹⁶⁸, and Leu¹⁶⁹ in the $\beta 6/\beta 7$ loop and Trp¹⁹⁴ in the $\beta 7/\beta 8$ loop consistently interact with the bound inhibitor. Structures of the SrtB sortase have also been determined in complex with small-molecule inhibitors. To aid development of aryl (β -amino)ethyl ketone (AAEK)-based inhibitors, Maresso and colleagues solved the crystal structures of *B. anthracis* SrtB bound to two different AAEK compounds.^[17] Similar to **2-salt** and the benzisothiazolinone compound, AAEK covalently modifies the active site cysteine residue (Cys²³³ in SrtB). Interestingly, while AAEK does not make specific contacts with residues within the active site loops, the compound nevertheless induces ordering of the $\beta 7/\beta 8$ loop and partial disordering of the $\beta 6/\alpha 5$ loop (SrtB equivalent of the $\beta 6/\beta 7$ loop). Combined, structural studies of sortase–inhibitor complexes reveal that sortase inhibitors could modulate the active site loops dynamics, and high-affinity binding might be achieved by maximizing contacts with the residues within the active site loops.

Rational approaches were employed to identify pyridazinone analogues with improved inhibitory activity. Concurrently, we also sought to increase the aqueous solubility of the inhibitors by adding polar substituents to sites on the inhibitor that based on the structure of the complex are surface-exposed. This was done to diminish the capacity of the inhibitor to cross the host cell membrane where it could cause undesirable off-target effects. As described in the section 3, analogues of **2–10** containing a single alteration at site

R2 to R6 were computationally evaluated for their ability to bind SrtA using the structure of the complex as a template. This identified substituents at each site that improved binding affinity, which were then tested in combination using docking calculations that employed the relaxed complex scheme approach to account for protein flexibility. Analogues that scored the highest in this analysis were then synthesized and experimentally tested. This led to a total of seven new analogues that have improved inhibitory activity against SrtA. Modification of the ortho-positions of the 2-phenyl ring have a large impact on activity and solubility. Based on the structure of the complex, substituents at these sites either project into the solvent (R4) or contact hydrophobic residues in the active site loop (R6). Compounds **2–51** to **2–53** selectively modify position R6 on the scaffold, and show improved activity when bulkier fluoro (**2–51**) or O-methyl groups (**2–53**) are added, resulting in nine- and twofold improvements in inhibitory activity, respectively. Based on the structure, these modifications fill a hydrophobic pocket on the enzyme that is formed by non-polar side chains originating from the $\beta 6/\beta 7$ loop (Val¹⁶⁶, Val¹⁶⁸, and Leu¹⁶⁹), the $\beta 7/\beta 8$ loop (Val¹⁹³), and the underlying beta sheet (Ile¹⁸² in strand $\beta 7$). Interestingly, only small improvements are observed for **2–52**, presumably because this analogue adds a methyl group at site R6 that may be too small to adequately fill the pocket. In contrast, while a fluoro group is slightly smaller than a methyl group, it is capable of forming multipolar contacts with the protein in addition to hydrophobic interactions,^[56] which might explain the bigger improvement in activity of **2–51** over **2–52**. Similar to site R6, the R4 site is in an ortho-position, but it is located on the opposite side of the phenyl ring where it is surface-exposed and projected toward an anionic patch on the enzyme that is formed by the side chains of Glu¹⁰⁵ and Asp¹⁷⁰. The positioning of the R4 substituent in the structure of the complex is compatible with the inhibitory properties of compound **2–54**, which exhibits a ~threefold reduction in its IC₅₀ relative to the lead molecule. This is because this analogue contains an amidine substituent at site R4 which can presumably form favorable electrostatic interactions. Notably, the addition of a polar amidine substituent at this site substantially decreases the cLogP score as compared to the parent molecule, suggesting that polar substituent addition to site R4 is a viable strategy for improving inhibitor solubility.

Based on the docking studies, a total of 12 analogues containing alterations at site R2 were synthesized and tested experimentally. Based on the structure of the complex, R2 substituents rest on a surface-exposed groove that is located in between the $\beta 7/\beta 8$ and $\beta 2/H1$ loops. The addition of hydroxyl bearing 2-hydroxyethoxy (**2–55**) and 3-hydroxypropoxy (**2–56**) at site R2 led to 6.8- and 1.8-fold improved activity, respectively. Although the co-ordinates of the R2 substituent (4-ethoxy) are poorly defined in the structure of SrtA:**2-salt**, the improved binding of these molecules may result from

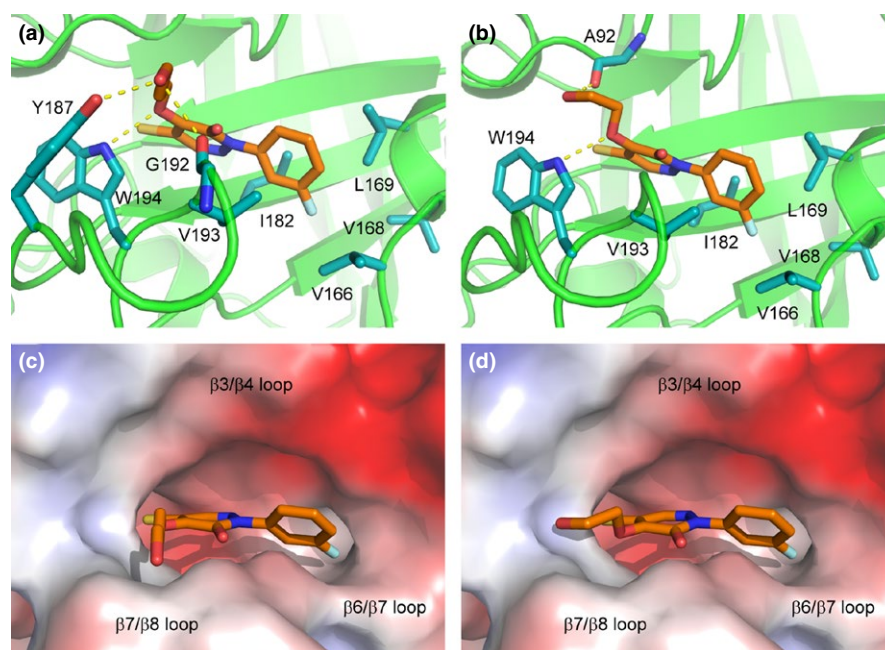
their ability to form additional hydrogen bonds via their hydroxyl group to residues within the β 2/H1 or β 7/ β 8 loops. Interestingly, this poorly defined subsite on SrtA does not accommodate large carboxylic acid and amide substituents at site R2, as analogues containing these modifications (**2–57** to **2–60**) have increased IC_{50} values. In addition to *S. aureus* SrtA, we also tested each compound's ability to inhibit the activity of the SrtA sortase enzyme from *B. anthracis* (Ba-SrtA), another important human pathogen that causes anthrax disease.^[57] SrtA and Ba-SrtA recognize related LPXTG sorting signals and their active sites adopt similar, but non-identical atomic structures.^[47] As with SrtA, modifications at sites R2 and R6 in the lead molecule led to improved inhibitory activity. The greatest gains in activity occur when the R6 site is modified with a methoxy group (**2–53**) (eightfold improved activity as compared to the lead molecule). However, distinct trends in the SAR data for SrtA and Ba-SrtA are evident. For example, in contrast to SrtA, modifying the R4 site with amidine led to an increase in IC_{50} . This is presumably because the *bacillus* enzyme lacks the aforementioned acidic residues that are presumed to stabilize binding to SrtA. Combined, experimental testing of the computationally optimized analogues of **2–10** substantiates the importance of three sites on the pyridazinone scaffold (R2, R4 and R6), which when changed individually improve inhibitory activity against SrtA up to ninefold.

Modifying two sites on the pyridazinone scaffold yielded the most potent sortase inhibitor, compound **2–62** (2-(3-fluorophenyl)-4-(3-hydroxypropoxy)-5-mercaptopyridazin-3(2*H*)-one). It is 70 times more active than the lead compound (IC_{50} of 21 nM) and contains 3-hydroxypropoxy and fluoro groups at sites R2 and R6, respectively. Its activity indicates that modification of sites R2 and R6 can have an additive effect, as individually these alterations are predicted to improve

binding 63-fold (6.8-fold for site R2 and ninefold for site R6). The docking pose of **2–62** suggests that its improved binding can be attributed to an increase in the van der Waals contact surface with the enzyme afforded by addition of a fluoro group at position R6 (~10 Å² increase in buried surface area) (Figure 7a,c). In addition, binding may be aided by new favorable interactions to the β 7/ β 8 loop formed from the terminal hydroxyl on the O(CH₂)₃OH group, as it is positioned to donate and accept a hydrogen bond from the backbone carbonyl oxygen of Gly¹⁹² and side chain hydroxyl group of Tyr¹⁸⁷, respectively. Moreover, in the **2–62** docking pose the oxygen at the R2 site closest to the pyridazinone ring is positioned to accept a hydrogen bond from the ϵ NH group in the indole ring of Trp¹⁹⁴. Interestingly, a close analogue of **2–62** that contains O(CH₂)₂OH at position R2 instead of O(CH₂)₃OH (compound **2–61**) is ~20 times less potent than **2–62**. Insight into its reduced potency is provided by its docking pose, which reveals that its shorter R2 side chain does not favorably hydrogen bond with Tyr¹⁸⁷ and Gly¹⁹², but instead forms a single hydrogen bond to the backbone oxygen of Ala⁹² located in the β 2/H1 loop (Figure 7b,d).

Because the pyridazinone molecules covalently inactivate sortase, the IC_{50} values reported in Table 2 may not accurately define each inhibitor's potency, as this parameter does not reveal the rate at which the small molecules modify and inactivate the enzyme. We therefore measured the k_{inact} and K_I parameters for **2–17**, **2–54**, and **2–62**, which were also tested using the cellular assay. As reported in Table 3, **2–62** has the highest inactivation efficiency ($k_{inact}/K_I = 0.003 \mu\text{M}^{-1}\text{s}^{-1}$), which is consistent with it having the lowest measured IC_{50} value when it is pre-incubated with the enzyme for 1 hr (Table 2). Although **2–10** was not tested due to its tendency to oxidize into **2–17**, presumably

FIGURE 7 Docking poses of compounds **2–61** and **2–62**. Expanded view of the active site showing interactions between the protein and compound **2–62** (a, c) and compound **2–61** (b, d). In (a) and (b), residues that contact the compound are shown as cyan sticks. Hydrogen bonds are indicated by yellow dotted lines. In (c) and (d), the protein solvent accessible surface is shown and colored by its electrostatic properties from acidic (red) to basic (blue)





the ~10-fold lower IC_{50} of **2-17** as compared to **2-10** is caused by a difference in their k_{inact} values. This is because it is expected that **2-17** will have a higher k_{inact} value as it inactivates sortase's Cys¹⁸⁴ residue via a thiol-disulfide exchange mechanism, whereas **2-10** inactivates sortase via a slower thiol–thiol oxidation process. Notably, **2-62** inactivates SrtA significantly more efficiently than previously reported diazoketone or chloromethylketone containing peptidomimics, which exhibited k_{inact}/K_I values of $0.0004 \mu\text{M}^{-1}\text{s}^{-1}$ and $0.0009 \mu\text{M}^{-1}\text{s}^{-1}$, respectively.^[58] This is presumably a result of the higher reactivity of the sulphhydryl group, which we have shown modifies the active site cysteine residue (Figure 3). Importantly, the SrtA inhibitors are capable of reducing protein display in intact *S. aureus* cells, as incubating analogues **2-17**, **2-54**, and **2-62** with bacterial cell cultures dramatically reduces SpA reporter protein display (Figure 5b). Interestingly, although **2-62** is the most potent compound in vitro based on its k_{inact}/K_I and IC_{50} values, **2-54** is nonetheless more effective than **2-17** or **2-62** at inhibiting SpA display in intact cells. This could be due to the positive charge on the amidine group in **2-54**, which may better allow it to traverse the cell wall as compared to the less polar **2-17** and **2-62** molecules. This idea is consistent with the finding that **2-17** and **2-62** do not exhibit dose-dependent activity in the cellular assay when their concentration is increased from 50 to 100 μM . Presumably, their higher cLogP values as compared to **2-54** cause them to be less soluble in the growth media used in cellular assay, thereby limiting the effective inhibitor concentration that can be achieved at the cell surface. In general, our inhibitors are less active in the cellular assay as compared to the in vitro assay. It is conceivable that their effective concentration in the cellular assay is reduced because they non-specifically interact with the bacterial cell wall, or because they interact with components that are uniquely present in the growth media (e.g., secreted proteins). In particular, the presence of low molecular weight thiol-containing compounds in the media (e.g., glutathione or coenzyme A) could inactivate the inhibitors by covalently modifying their thiol group. Importantly, although complete disruption of display was not achieved at 100 μM , the in vitro and cellular potencies of our compounds are similar to, or better than, recently described SrtA inhibitors that are efficacious in treating *S. aureus* infections in a mouse model.^[49]

5 | CONCLUSIONS

In summary, using NMR spectroscopy, mass spectrometry and a designed soluble analogue, we have determined the mechanism through which pyridazinone-based small molecules inhibit the *S. aureus* SrtA enzyme. We demonstrate

that these inhibitors partially mimic SrtA's natural substrate by partially inducing a disordered to ordered conformational change in the $\beta 6/\beta 7$ active site loop. Using computational and synthetic chemistry approaches, several second-generation inhibitors have been produced that have increased inhibitory activity, both in vitro and on the bacterial cell surface. At present, two SrtA inhibitors have now been reported that are efficacious in treating potentially lethal *S. aureus* infections in animal models. These molecules include, (Z)-3-(2,5-dimethoxyphenyl)-2-(4-methoxyphenyl) acrylonitrile (DMMA) and 3-(4-pyridinyl)-6-(2-sodiumsulfonatephenyl)[1,2,4]triazolo[3,4-b][1,3,4]thiadiazole (triazolothiadiazole), which were efficacious when dosed at 20 and 40 mg of compound per kg of animal, respectively.^[49,59] The **2-62** pyridazinone compound reported in this paper has a lower IC_{50} than these molecules; **2-62** has an $IC_{50} = 0.02 \mu\text{M}$, versus IC_{50} values of 9.2 and 9.3 μM for DMMA and triazolothiadiazole, respectively. This suggests that **2-62** and related pyridazinone molecules are potential candidates for further development into anti-infective agents. Such new therapeutics are needed, as many microbial pathogens are increasingly becoming resistant to current antibiotic therapies.

ACKNOWLEDGMENTS

This research was supported by funding from the National Institutes of Health (AI52217 to R.T.C. and M.E.J.; and GM31749 to J.A.M.). A.H.C. was supported by the UCLA Chemistry Biology Interface Training program (NIH T32GM008496). B.R.A. was supported by the UCLA-MBI Whitcome Pre-Doctoral Training Grant. Additional support at UCSD has been provided by the National Science Foundation, the Howard Hughes Medical Institute, the Center for Theoretical Biological Physics, the National Biomedical Computation Resource, and the NSF Supercomputer Centers. Mass Spectrometry Instrumentation was made available through the support of Greg Khitrov (University of California, Los Angeles Molecular Instrumentation Center—Mass Spectrometry Facility in the Department of Chemistry). The mass spectrometry data were collected through a project described and supported by Grant Number S10-RR025631 from the National Center for Research Resources.

CONFLICT OF INTEREST

There are no conflict of interests.

NOTE

^a Center for Disease Control and Prevention. 2013. Antibiotic Resistance Threats in the United States, 2013. <http://www.cdc.gov/drugresistance/threat-report-2013/>.

REFERENCES

- [1] F. D. Lowy, *N. Engl. J. Med.* **1998**, *339*, 520.
- [2] D. J. Pallin, D. J. Egan, A. J. Pelletier, J. A. Espinola, D. C. Hooper, C. A. Camargo Jr, *Ann. Emerg. Med.* **2008**, *51*, 291.
- [3] L. F. McCaig, L. C. McDonald, S. Mandal, D. B. Jernigan, *Emerg. Infect. Dis.* **2006**, *12*, 1715.
- [4] K. J. Welsh, A. N. Abbott, E. M. Lewis, J. M. Gardiner, M. C. Kruzell, C. T. Lewis, J. F. Mohr, A. Wanger, L. Y. Armitage, *J. Clin. Microbiol.* **2010**, *48*, 894.
- [5] F. M. Marty, W. W. Yeh, C. B. Wennersten, L. Venkataraman, E. Albano, E. P. Alyea, H. S. Gold, L. R. Baden, S. K. Pillai, *J. Clin. Microbiol.* **2006**, *44*, 595.
- [6] Y. Ikeda-Dantsuji, H. Hanaki, F. Sakai, K. Tomono, Y. Takesue, J. Honda, Y. Nonomiya, A. Suwabe, O. Nagura, K. Yanagihara, H. Mikamo, K. Fukuchi, M. Kaku, S. Kohno, C. Yanagisawa, T. Nakae, K. Yoshida, Y. Niki, *J. Infect. Chemother.* **2011**, *17*, 45.
- [7] W. W. Navarre, O. Schneewind, *Microbiol. Mol. Biol. Rev.* **1999**, *63*, 174.
- [8] T. J. Foster, J. A. Geoghegan, V. K. Ganesh, M. Hook, *Nat. Rev. Microbiol.* **2014**, *12*, 49.
- [9] S. K. Mazmanian, G. Liu, E. R. Jensen, E. Lenoy, O. Schneewind, *Proc Natl Acad Sci U S A* **2000**, *97*, 5510.
- [10] S. Cascioferro, M. Totsika, D. Schillaci, *Microb. Pathog.* **2014**, *77*, 105.
- [11] T. Spirig, E. M. Weiner, R. T. Clubb, *Mol. Microbiol.* **2011**, *82*, 1044.
- [12] S. K. Mazmanian, G. Liu, H. Ton-That, O. Schneewind, *Science* **1999**, *285*, 760.
- [13] D. A. Rasko, V. Sperandio, *Nat. Rev. Drug Discov.* **2010**, *9*, 117.
- [14] S. Escaich, *Curr. Opin. Chem. Biol.* **2008**, *12*, 400.
- [15] N. Suree, M. E. Jung, R. T. Clubb, *Mini Rev. Med. Chem.* **2007**, *7*, 991.
- [16] D. Zhulenkova, Z. Rudevica, K. Jaudzems, M. Turks, A. Leonchiks, *Bioorg. Med. Chem.* **2014**, *22*, 5988.
- [17] A. W. Maresso, R. Wu, J. W. Kern, R. Zhang, D. Janik, D. M. Missiakas, M. E. Duban, A. Joachimiak, O. Schneewind, *J. Biol. Chem.* **2007**, *282*, 23129.
- [18] R. Zhang, R. Wu, G. Joachimiak, S. K. Mazmanian, D. M. Missiakas, P. Gornicki, O. Schneewind, A. Joachimiak, *Structure* **2004**, *12*, 1147.
- [19] N. Suree, S. W. Yi, W. Thieu, M. Marohn, R. Damoiseaux, A. Chan, M. E. Jung, R. T. Clubb, *Boorg. Med. Chem.* **2009**, *17*, 7174.
- [20] U. Ilangovan, H. Ton-That, J. Iwahara, O. Schneewind, R. T. Clubb, *Proc. Natl. Acad. Sci. USA* **2001**, *98*, 6056.
- [21] F. Delaglio, S. Grzesiek, G. W. Vuister, G. Zhu, J. Pfeifer, A. Bax, *J. Biomol. NMR* **1995**, *6*, 277.
- [22] D. S. Garrett, R. Powers, A. M. Gronenborn, G. M. Clore, *J. Magn. Reson.* **1991**, *95*, 214.
- [23] R. Keller, *The Computer Aided Resonance Assignment Tutorial*, CATINA Verlag, Goldau, Switzerland **2004**.
- [24] J. Cavanagh, W. J. Fairbrother, A. G. Palmer, N. J. Skelton, *Protein NMR Spectroscopy*, 2nd ed., Elsevier Science and Technology, San Diego, CA **2006**.
- [25] Q. Teng, *Structural Biology: Practical NMR Applications*, Springer Verlag, New York **2005**.
- [26] Y. Shen, F. Delaglio, G. Cornilescu, A. Bax, *J. Biomol. NMR* **2009**, *44*, 213.
- [27] G. W. Vuister, A. Bax, *J. Am. Chem. Soc.* **1993**, *115*, 7772.
- [28] T. Herrmann, P. Guntert, K. Wuthrich, *J. Biomol. NMR* **2002**, *24*, 171.
- [29] T. Herrmann, P. Guntert, K. Wuthrich, *J. Mol. Biol.* **2002**, *319*, 209.
- [30] C. D. Schwieters, J. J. Kuszewski, N. Tjandra, G. M. Clore, *J. Magn. Reson.* **2003**, *160*, 65.
- [31] Y. Zong, T. W. Bice, H. Ton-That, O. Schneewind, S. V. Narayana, *J. Biol. Chem.* **2004**, *279*, 31383.
- [32] N. Suree, C. K. Liew, V. A. Villareal, W. Thieu, E. A. Fadeev, J. J. Clemens, M. E. Jung, R. T. Clubb, *J. Biol. Chem.* **2009**, *284*, 24465.
- [33] R. Koradi, M. Billeter, K. Wuthrich, *J. Mol. Graph.* **1996**, *14*(51–5), 29.
- [34] W. L. DeLano, *The PyMOL Molecular Graphics System*. The PyMOL Molecular Graphics System, DeLano Scientific LLC, Palo Alto, CA **2006**.
- [35] G. M. Sastry, M. Adzhigirey, T. Day, R. Annabhimoju, W. Sherman, *J. Comput. Aided Mol. Des.* **2013**, *27*, 221.
- [36] T. A. Halgren, R. B. Murphy, R. A. Friesner, H. S. Beard, L. L. Frye, W. T. Pollard, J. L. Banks, *J. Med. Chem.* **2004**, *47*, 1750.
- [37] R. A. Friesner, J. L. Banks, R. B. Murphy, T. A. Halgren, J. J. Klicic, D. T. Mainz, M. P. Repasky, E. H. Knoll, M. Shelley, J. K. Perry, D. E. Shaw, P. Francis, P. S. Shenkin, *J. Med. Chem.* **2004**, *47*, 1739.
- [38] R. A. Friesner, R. B. Murphy, M. P. Repasky, L. L. Frye, J. R. Greenwood, T. A. Halgren, P. C. Sanschagrin, D. T. Mainz, *J. Med. Chem.* **2006**, *49*, 6177.
- [39] J. Wang, W. Wang, P. A. Kollman, D. A. Case, *J. Mol. Graph. Model.* **2006**, *25*, 247.
- [40] J. Wang, R. M. Wolf, J. W. Caldwell, P. A. Kollman, D. A. Case, *J. Comput. Chem.* **2004**, *25*, 1157.
- [41] W. D. Cornell, P. Cieplak, C. I. Bayly, P. A. Kollman, *J. Am. Chem. Soc.* **1993**, *115*, 9620.
- [42] M. J. Frisch, G. W. Trucks, H. B. Schlegel, G. E. Scuseria, M. A. Robb, J. R. Cheeseman, G. Scalmani, V. Barone, B. Mennucci, G. A. Petersson, H. Nakatsuji, M. Caricato, X. Li, H. P. Hratchian, A. F. Izmaylov, J. Bloino, G. Zheng, J. L. Sonnenberg, M. Hada, M. Ehara, K. Toyota, R. Fukuda, J. Hasegawa, M. Ishida, T. Nakajima, Y. Honda, O. Kitao, H. Nakai, T. Vreven, J. A. Montgomery, Jr., J. E. Peralta, F. Ogliaro, M. Bearpark, J. J. Heyd, E. Brothers, K. N. Kudin, V. N. Staroverov, R. Kobayashi, J. Normand, K. Raghavachari, A. Rendell, J. C. Burant, S. S. Iyengar, J. Tomasi, M. Cossi, N. Rega, J. M. Millam, A. Rendell, M. Klene, J. E. Knox, J. B. Cross, V. Bakken, C. Adamo, J. Jaramillo, R. Gomperts, R. E. Stratmann, O. Yazyev, A. J. Austin, R. Cammi, C. Pomelli, J. W. Ochterski, R. L. Martin, K. Morokuma, V. G. Zakrzewski, G. A. Voth, P. Salvador, J. J. Dannenberg, S. Dapprich, A. D. Daniels, O. Farkas, J. B. Foresman, J. V. Ortiz, J. Cioslowski, D. J. Fox, *Gaussian 09*, Revision D.01, Gaussian, Inc., Wallingford, CT, **2013**.
- [43] A. H. Chan, J. Wereszczynski, B. R. Amer, S. W. Yi, M. E. Jung, J. A. McCammon, R. T. Clubb, *Chem. Biol. Drug Des.* **2013**, *82*, 418.
- [44] K. Lindorff-Larsen, S. Piana, K. Palmo, P. Maragakis, J. L. Klepeis, R. O. Dror, D. E. Shaw, *Proteins* **2010**, *78*, 1950.
- [45] J. C. Phillips, R. Braun, W. Wang, J. Gumbart, E. Tajkhorshid, E. Villa, C. Chipot, R. D. Skeel, L. Kale, K. Schulten, *J. Comput. Chem.* **2005**, *26*, 1781.

- [46] S. Pronk, S. Pall, R. Schulz, P. Larsson, P. Bjelkmar, R. Apostolov, M. R. Shirts, J. C. Smith, P. M. Kasson, D. van der Spoel, B. Hess, E. Lindahl, *Bioinformatics* **2013**, *29*, 845.
- [47] E. M. Weiner, S. Robson, M. Marohn, R. T. Clubb, *J. Biol. Chem.* **2010**, *285*, 23433.
- [48] R. A. Copeland, *Evaluation of Enzyme Inhibitors in Drug Discoveries: A Guide for Medicinal Chemists and Pharmacologists*, John Wiley & Sons, New Jersey **2005**.
- [49] J. Zhang, H. Liu, K. Zhu, S. Gong, S. Dramsi, Y. T. Wang, J. Li, F. Chen, R. Zhang, L. Zhou, L. Lan, H. Jiang, O. Schneewind, C. Luo, C. G. Yang, *Proc. Natl. Acad. Sci. USA* **2014**, *111*, 13517.
- [50] S. P. Crouch, R. Kozlowski, K. J. Slater, J. Fletcher, *J. Immunol. Methods* **1993**, *160*, 81.
- [51] J. H. Lin, A. L. Perryman, J. R. Schames, J. A. McCammon, *Biopolymers* **2003**, *68*, 47.
- [52] R. E. Amaro, R. Baron, J. A. McCammon, *Aided Mol. Des.* **2008**, *22*, 693.
- [53] L. A. Marraffini, A. C. Dedent, O. Schneewind, *Microbiol. Mol. Biol. Rev.* **2006**, *70*, 192.
- [54] F. Falugi, H. K. Kim, D. M. Missiakas, O. Schneewind, *MBio* **2013**, *4*, e00575.
- [55] S. Cascioferro, D. Raffa, B. Maggio, M. V. Raimondi, D. Schillaci, G. Daidone, *J. Med. Chem.* **2015**, *58*, 9108.
- [56] K. Muller, C. Faeh, F. Diederich, *Science* **2007**, *317*, 1881.
- [57] M. Mock, A. Fouet, *Annu. Rev. Microbiol.* **2001**, *55*, 647.
- [58] C. J. Scott, A. McDowell, S. L. Martin, J. F. Lynas, K. Vandebroek, B. Walker, *Biochem J.* **2002**, *366*, 953.
- [59] K. B. Oh, K. W. Nam, H. Ahn, J. Shin, S. Kim, W. Mar, *Biochem. Biophys. Res. Commun.* **2010**, *396*, 440.

SUPPORTING INFORMATION

Additional Supporting Information may be found online in the supporting information tab for this article.

How to cite this article: Chan AH, Yi SW, Weiner EM, et al. NMR structure-based optimization of *Staphylococcus aureus* sortase A pyridazinone inhibitors. *Chem Biol Drug Des.* 2017;00:1–18. <https://doi.org/10.1111/cbdd.12962>